Journal of Power Sources 229 (2013) 22–31

Contents lists available at SciVerse ScienceDirect

Journal of Power Sources

journal homepage: www.elsevier.com/locate/jpowsour

Alkaline electrolysis cell at high temperature and pressure of 250 °C and 42 bar

Frank Allebrod*, Christodoulos Chatzichristodoulou, Mogens B. Mogensen

Technical University of Denmark, Department of Energy Conversion and Storage, Frederiksborgvej 399, P.O. Box 49, 4000 Roskilde, Denmark

HIGHLIGHTS

- A new type of an alkaline electrolysis cells has been developed.
- Metal foam based gas diffusion electrodes with Ag electro-catalyst were used.
- Potassium hydroxide as electrolyte was immobilized in a porous $SrTiO_3$ structure.
- The cells have shown to operate at temperatures up to 250 °C at 42 bar.
- Current densities of 1.0 A cm^{-2} and 2.0 A cm^{-2} have been measured at 1.5 V and 1.75 V.

ARTICLE INFO

Article history:
Received 13 July 2012
Received in revised form
22 October 2012
Accepted 16 November 2012
Available online 1 December 2012

Keywords:
Alkaline electrolysis
High temperature
High pressure
Gas diffusion electrodes
Metal foam

ABSTRACT

A new type of alkaline electrolysis cells with nickel foam based gas diffusion electrodes and KOH (aq) immobilized in mesoporous $SrTiO_3$ has been developed and tested at temperatures and pressures up to 250 °C and 42 bar, respectively. Current densities of 1.0 A cm^{-2} have been measured at a cell voltage of 1.5 V without the use of expensive noble metal catalysts. High electrical efficiency and current density combined with relatively small production costs may lead to both reduced investment and operating costs for hydrogen and oxygen production.

1. Introduction

Energy from renewable sources is becoming an increasingly important part of the energy supply system worldwide. Besides the obvious advantages of renewable energy sources, like CO_2 free or neutral energy production, some indisputable disadvantages have to be overcome towards a sustainable energy supply system [1]. The fluctuation of the wind speed and solar radiation, for example, leads to periods with excess or deficit of available energy. It is therefore necessary to develop energy storage systems with high efficiency and reliability, as well as low cost. The production of hydrogen by means of electrolysis of water during times of energy excess, followed by conversion of the produced hydrogen to electricity during periods of energy deficit is a promising possibility [2]. Alkaline electrolysis has proven to be reliable and efficient some decades ago [3], but further cost reduction along with increased efficiency is still necessary in order to make it commercially attractive. A significant reduction of the investment costs may be achieved by increasing the operational pressure of the electrolyzer as this will result in the production of pressurized hydrogen (and oxygen), thereby eliminating or reducing the cost of the compressor. Furthermore, it has been estimated that the energy demand for pressurization by the electrolyzer is ca. 5% less than for pressurization by common compressors, leading to reduced operation cost for the system [4].

A substantial step towards higher efficiencies can be made by increasing the operational temperature from the conventionally used temperature of about 100 °C to temperatures as high as 264 °C, where a current density of 200 mA cm^{-2} has been demonstrated at a cell voltage of 1.43 V [5]. Another substantial step forward has been made by Divisek et al. by the use of Raney activated electrodes and zero-gap electrodes, thereby achieving a current density of 400 mA cm^{-2} at a cell voltage of ca. 1.55 V at 100 °C and pressures between 1 and 5 bar [3].

* Corresponding author. Tel.: +45 21330321; fax: +45 46775858.
E-mail addresses: fkal@dtu.dk (F. Allebrod), ccha@dtu.dk (C. Chatzichristodoulou), momo@dtu.dk (M.B. Mogensen).

0378-7753/$ – see front matter © 2012 Elsevier B.V. All rights reserved.
http://dx.doi.org/10.1016/j.jpowsour.2012.11.105

1.1. Alkaline electrolysis

An alkaline electrolysis cell consists of four major components; the electrolyte, which is commonly potassium hydroxide (KOH) in high concentrations (usually above 25 wt%), the cathode, the anode, and a solid barrier (diaphragm). The solid barrier is separating the produced gases to avoid recombination and furthermore needs to be permeable to hydroxide ions and water; it is used in all types of alkaline electrolysis cells (conventional, zero-gap, immersed cells, or gas diffusion electrode type alkaline electrolyzers) [6,7]. Hydrogen evolution takes place at the cathode, where the electrons are provided for the decomposition of water. The hydroxide ions are decomposed at the anode, where oxygen evolution takes place under the formation of water. The basic reactions of the decomposition of water in an alkaline electrolyzer are given by Equations (1)–(3).

$$\text{Anode}: 2OH^- \rightarrow \frac{1}{2}O_2 + H_2O + 2e^- \quad (1)$$

$$\text{Cathode}: 2H_2O + 2e^- \rightarrow H_2 + 2OH^- \quad (2)$$

$$\text{Total}: H_2O \rightarrow H_2 + \frac{1}{2}O_2 \quad (3)$$

The cell voltage, U_{cell}, that has to be applied to produce hydrogen and oxygen with a given rate depends on the operating temperature [8] and pressure [4] as well as on a number of other factors such as the electro-catalyst material and microstructure [9]. Furthermore, the right choice of electrolyte concentration for a specific temperature [10], and a high specific surface area of the electrodes are important factors. Major losses are defined as cathodic overvoltage, η_{H_2}, for the hydrogen evolution reaction, HER, the anodic overvoltage, η_{O_2}, for the oxygen evolution reaction, OER, and ohmic losses in the electrolyte. The ohmic losses are relatively small at low current densities, but become significant at industrially relevant current densities of 200 mA cm^{-2} or more, especially if significant bubble formation takes place [11].

1.2. Thermodynamic considerations

The reversible (or equilibrium) cell voltage, E_{rev}, is the minimal voltage at which electrolysis of H_2O is possible and can be calculated by equation, where ΔG_f is the Gibbs free energy of the reaction, n is the number of electrons involved in the reaction, and F is Faraday's constant (96,485 C mol^{-1}). At standard conditions it is 1.229 V with the Gibbs free energy of formation at standard conditions $\Delta G_f^0 = -237.178$ kJ mol^{-1} [12].

$$E_{rev} = \frac{-\Delta G_f}{nF} \quad (4)$$

The total energy demand for the reaction corresponds to the thermoneutral voltage, E_{tn}, and can be calculated from the enthalpy of formation, ΔH_f, as shown by Equation (5). The thermoneutral voltage $E_{tn,0}$ at standard temperature and pressure (STP, 25 °C, 101.325 kPa) is 1.481 V with the standard enthalpy of formation $\Delta H_f^0 = -285.840$ kJ mol^{-1} [12].

$$E_{tn} = \frac{-\Delta H_f}{nF} \quad (5)$$

A comparison of the electrical energy demand, the total energy demand and the heat demand for water electrolysis at standard pressure is shown in Fig. 1 with thermodynamic data obtained from FactSage [12]. It is shown that the electrical energy demand for water electrolysis decreases with increasing temperature, while heat demand rises and the total energy demand is almost constant (but different) both for the liquid and the gaseous phase.

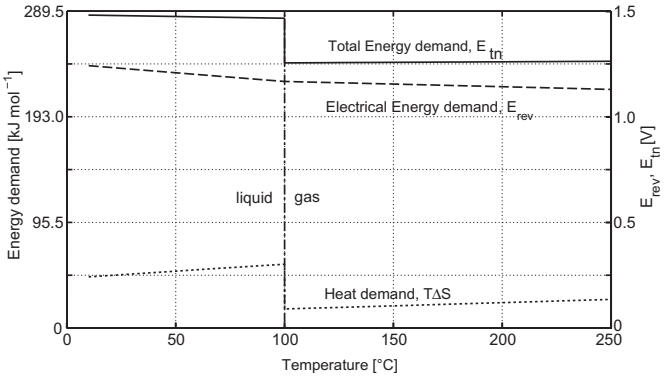

Fig. 1. Temperature dependence of the total energy demand, ΔH_f (full line), the electrical energy demand, ΔG_f (dashed line), and the heat demand $T \cdot \Delta S_f$ (dotted) for water ($T \leq 100$ °C) and steam ($T \geq 100$ °C) electrolysis at 1 bar using data from FactSage [12].

As it is not common to perform electrolysis at standard conditions, it is necessary to know both the influence of pressure and temperature to the reversible cell voltage. The reversible cell voltage as a function of temperature and pressure, $E_{rev(t,p)}$, can be calculated by Equation (6), where R is the Gas constant (8.3144621 J mol^{-1} K^{-1}), a_{H_2} is the hydrogen activity, a_{O_2} is the oxygen activity, a_{H_2O} is the activity of water and T is the temperature in Kelvin.

$$E_{rev(t,p)} = \frac{-\Delta G_f}{n \cdot F} = \frac{-\Delta G_f^0}{n \cdot F} + \frac{RT}{nF} \ln\left(\frac{a_{H_2} a_{O_2}^{\frac{1}{2}}}{a_{H_2O}}\right) \quad (6)$$

$E_{rev(t,p)}$ can also be obtained from steam tables or CALPHAD (Computer Coupling of Phase Diagrams and Thermochemistry) programs like FactSage [12] which include data for ΔG_f at elevated temperatures and pressures. A graph displaying the influence of the pressure and temperature to $E_{rev(t,p)}$ has been calculated by Equation (4) with data from FactSage and is shown in Fig. 2 (the partial pressure of H_2, O_2 and H_2O is assumed equal to the total pressure in this calculation). Important values are numerically extracted in

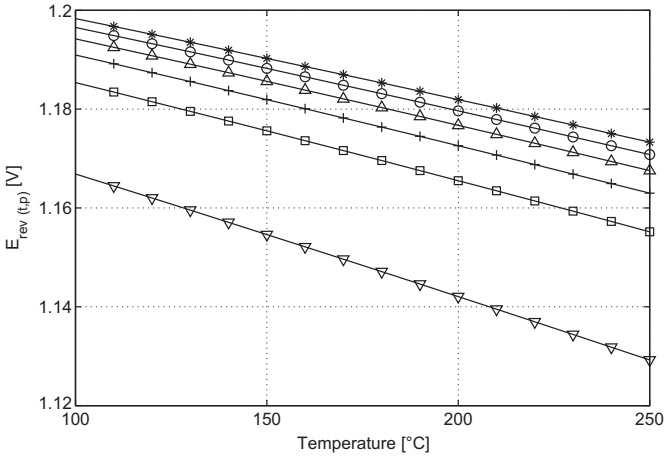

Fig. 2. Reversible cell voltage $E_{rev(t,p)}$ as a function of the temperature for steam electrolysis at pressures of 1 bar (∇), 10 bar (□), 20 bar (+), 30 bar (△), 40 bar (○) and 50 bar (★) (the partial pressure of H_2, O_2 and H_2O is assumed equal to the total pressure in this calculation).

Table 1. Furthermore, it should be noted that the reversible cell voltage of an alkaline electrochemical cell is also depending on the concentration of the electrolyte. Balej [13,14] has provided expressions for computing a_i and the reversible cell voltage as a function of the concentration, temperature and pressure of the electrolyte, said to be valid for temperatures between 25–200 °C. Since reliable data sets above 200 °C are not available, we have neglected the influence of the electrolyte concentration here.

1.3. Immobilization of electrolytes and gas diffusion electrodes

A porous structure in which the liquid electrolyte is immobilized by capillary forces can be used as a combination of diaphragm and electrolyte. In this case, the reduced free volume for the liquid electrolyte and the tortuosity of the porous structure are expected to result in a decrease in conductivity, and by that to an increase in ohmic losses. Nevertheless, the ohmic losses can be reduced by reducing the thickness of the porous structure. The determination of the conductivity of such structures is therefore important and can be measured with the van der Pauw technique as demonstrated by the authors [10]. A great advantage of immobilizing the electrolyte is the possibility to use gas diffusion electrodes (GDEs) for steam electrolysis at temperatures well above the boiling point of water, i.e. up to 250 °C in the work presented here, while the electrolyte remains in the liquid phase due to the higher boiling point of concentrated KOH (aq). At any given temperature, it is important to operate within an appropriate pressure range since too high pressures could cause condensation of steam (and thereby dilute the electrolyte or flood the GDE) while too low pressures could cause evaporation of the electrolyte (through which ohmic losses would increase). Further consequences of electrolyte evaporation could be disconnection of the circuit or the formation of open gas channels between cathode and anode. Phase transition lines between the liquid and liquid + gas phase for water and KOH solutions as a function of temperature and pressure have been presented in previous work [10].

Gas diffusion electrodes, similar to those used in high temperature solid oxide fuel cells (SOFC) and solid oxide electrolysis cells (SOEC) [15] allow electrolysis without the formation of bubbles. Bubble formation usually leads to increased ohmic losses due to area reduction and increased anodic and cathodic overpotentials due to reduced available electrode area in a traditional alkaline electrolyzer [16]. GDEs have to be highly electronic conductive to minimize ohmic losses, and porous to allow the produced gases to escape while steam flows into the cell towards the triple phase boundary, TPB, as shown in Fig. 3. Since the electrochemical reactions take place at the TPB, it is important that the TPB-length is as long as possible [17]. Nickel is known to be corrosion resistant in alkaline media and electro-catalytically active, hence it is often used as a base material for electrodes in alkaline electrolysis cells. Electro-catalysts for the OER [18,19] and HER [20,21] have been extensively studied for alkaline electrolysis. They are optimally placed at the TPB in order to achieve low overpotentials. Silver is known to be an excellent catalyst for the oxygen reduction reaction ORR in alkaline fuel cells [22,23] and can be considered as catalyst for the OER reaction as well. Co_3O_4 and Co-based spinel oxides are also known to be good electro-catalysts for the OER [24], while Raney-nickel and molybdenum [25] are preferred electro-catalysts for the HER. The anodic overpotential caused by the OER is usually dominating over the cathodic overpotential caused by the HER.

Table 1
Reversible cell voltage $E_{rev(t,p)}$ for steam electrolysis as a function of the system pressure and temperature calculated by Equation (4) with data from FactSage.

Temperature [°C]	System pressure [bar]					
	1	10	20	30	40	50
100	1.167	1.185	1.191	1.194	1.197	1.198
150	1.155	1.176	1.182	1.186	1.188	1.190
200	1.142	1.166	1.173	1.177	1.180	1.182
250	1.129	1.155	1.163	1.168	1.171	1.173

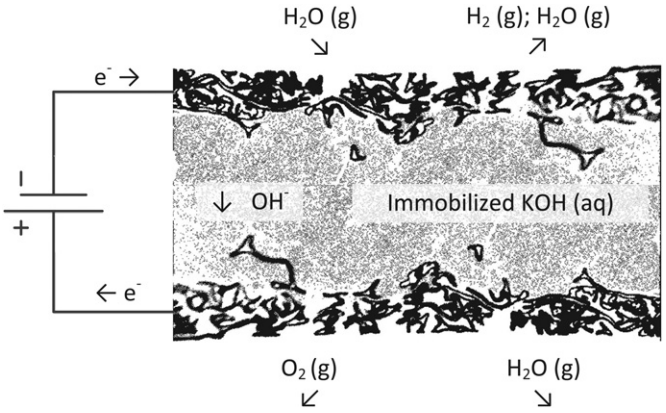

Fig. 3. Illustration of an alkaline electrolysis cell with KOH (aq) electrolyte immobilized in a porous matrix and gas diffusion electrodes.

Nickel foams are widely used [26] and have already been shown to work as a gas diffusion electrode for the oxygen reduction reaction ORR in an alkaline fuel cell [27]. More advanced metal foams have recently been developed from Alantum Europe GmbH, where metal alloy foams are obtained by a powder metallurgical process. Important material parameters, i.e. final composition, the specific surface area, and the pore size of the foam can be customized to the application [28].

2. Experimental

2.1. FobAEC – foam based alkaline electrolysis cells

A new type alkaline electrolysis cell and method to produce them has been developed [29]. Foam based alkaline electrochemical cells (FobAEC) are produced from metal foams delivered by Alantum Europe GmbH. Circular foam pieces with a diameter of 12 mm are stamped out of the foam sheets with a thickness of 1.0 mm for nickel foam, and 1.6 mm for Inconel 625 foam (Inconel 625 alloy composition is for example in wt%: Cr, 21.32; Mo, 8.58; Nb, 3.73; Al, 0.18; Ti, 0.16; Fe, 0.11; Si, 0.09; C, 0.053; Mn, 0.04; Mg, 0.01; Balance Ni [30]). The circular foam pieces were cleaned in ethanol; beside that, the foams were used as delivered. One or two foam layers are placed in a uni-axial press and 0.25–1.5 g $SrTiO_3$ powder is placed on top of the foam. One drop of an appropriate binder, i.e. MEK in 33% ethanol, has been mixed to 100 mg of the perovskite $SrTiO_3$ powder to obtain better adhesion of the powder particles during processing and sintering. Another one or two layers of foam are placed on top of the powder. The whole structure is pressed for 30 s with a pressure of 13.0 kN cm^{-2}. The cells have then been sintered in air at 450 °C for 2 h with a heating ramp of 100 K h^{-1} followed by a second sintering step in 9% H_2/Ar at 1000 °C for 6 h with a heating and cooling ramp of 50 K h^{-1}.

Mercury porosimetry analysis has been performed with an AutoPore IV 9500 porosimetry analyzer, since the porosity and pore size distribution of the $SrTiO_3$ structure is of high interest for the immobilization of the electrolyte. A sample for the pore size measurements has been produced similar to the FobAECs, but without the foams pressed to the surfaces.

Electrodeposition of silver has been performed to some of the cells in order to improve the performance of the anode for the OER after preparing the cells as described above. The electrodeposition was performed with a 0.1 M $AgNO_3$ + 1 M KNO_3 solution under N_2 atmosphere and stirring. Pulsed deposition with pulse/pause relation of 1 s/1 s and a potential difference of −3.0 V (vs a platinized Pt counter electrode) has been used to deposit the Ag particles on the foam with a Gamry type 600 or 3000 potentiostat. Scanning electron microscopy SEM has been used to analyze the surface and cross section of the FobAEC before and after measurements. Analysis of the impedance and voltammetry data was partly performed using the software Ravdav [31].

2.2. High temperature and pressure autoclave

A Parr autoclave Type 4760 with 600 ml volume and a PTFE (Polytetrafluoroethylene) liner was used to perform measurements under high pressure and at elevated temperatures as shown in Fig. 4. The autoclave was made of Inconel 600, which can withstand high temperatures and pressures as well as extremely caustic environments [32]. To perform electrochemical measurements, the autoclave was equipped with additional gas handling components and wire through-puts. Nitrogen from a 200 bar pressurized bottle was used for the pressurization of the Autoclave. The pressure in the autoclave was regulated with a needle valve. A J-type thermo-well was used to measure the temperature in the autoclave while a pressure gauge displayed the actual pressure. An additional digital pressure gauge allowed recording the pressure. The autoclave was insulated to avoid temperature gradients during the measurements.

2.3. Electrochemical measurements

Electrochemical measurements have been performed with a Gamry type 600 or 3000 potentiostat. Electrochemical impedance spectroscopy (EIS) has been used to determine the cell characteristics under polarization and at open circuit voltage (OCV). Cyclic voltammograms have been recorded to analyze the cell performance as a function of the applied cell voltage.

A cell holder was developed to allow electrochemical characterization of the FobAECs. It is important that the materials used for the tests will not suffer from severe corrosion or degradation due to the harsh conditions in the autoclave. Inconel was chosen where low electrical resistance was needed, PFA (Perfluoroalkoxy) or PTFE where insulating properties and chemical resistance was an issue. Fig. 5 shows the cross section of the cell holder that was used during the measurements. Nitinol (a nickel–titanium alloy) tension springs were used to apply a constant force between two Inconel tubes which acted as current collectors. Inconel screws attached to the Inconel tube acted as corrosion resistant connection points as well as mounting points for the Nitinol spring. PTFE O-rings ensured electronic insulation between the Inconel screws and the Nitinol springs. The FobAEC was placed in between two metal foams acting as current collectors (Inconel foam on the cathode, nickel on the anode). The produced gases could evolve through the Inconel tubes to the autoclave vessel. 5 mm holes on the side of the PFA tube fitting (Swagelock type PFA-820-6) ensured that the cell would not dry out during the performed measurements and allowed to connect a platinum wire to the centre of the cell (immobilized electrolyte) in order to perform measurements against this reference electrode (compare Section 2.4). The working electrode (WE) and the working sense (WS) of the potentiostat terminals were connected to the anodic side of the sample holder while the counter electrode (CE) and the reference (Ref) terminals were connected to the cathodic side of the sample holder.

The main intention of the presented work was to obtain performance data of the produced cells at temperatures close to 250 °C, but measurements at 100 °C and 200 °C have also been performed to analyze the influence of temperature. The cells have been kept in the aqueous electrolyte for at least 2 h prior to the measurements in order to soak up the electrolyte; the concentration

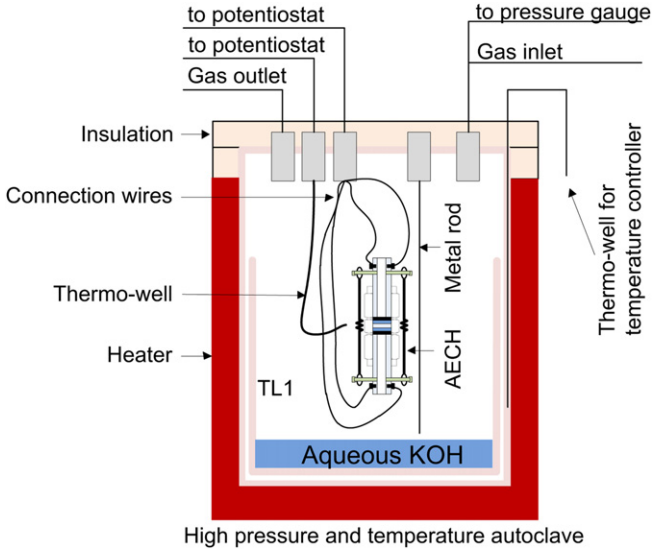

Fig. 4. Schematic description of the autoclave setup including heater and top insulation. A teflon liner TL1 protects the autoclave from the caustic environment. The alkaline electrochemical cell holder (AECH) is connected to a metal rod by an insulated wire (not shown). The diluted aq. KOH solution used to humidify the autoclave atmosphere is also shown. The temperature controller is connected to a thermo-well placed in between the heater and the autoclave.

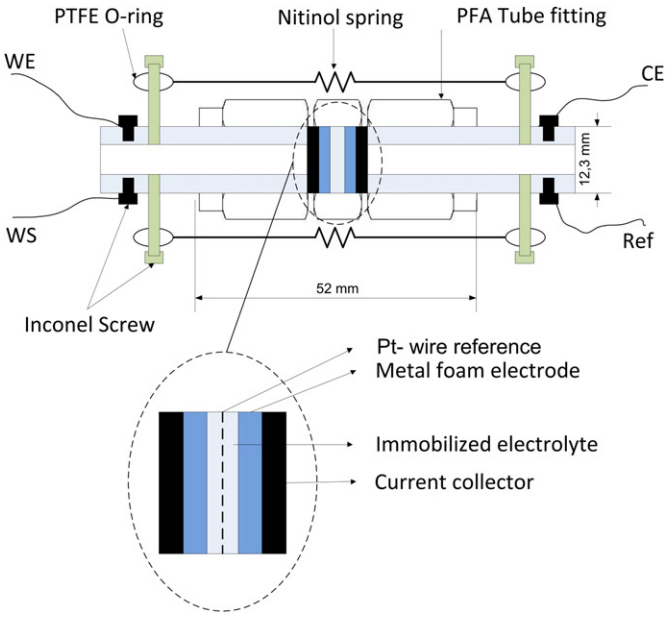

Fig. 5. Principal cross section of the Alkaline Electrolysis Cell Holder (AECH): The electrolysis cell is centred in the sample holder. A piece of metal foam acts as current collector. The Inconel tubes press the foam against the active electrode of the electrolysis cell. Nitinol springs are assembled to provide constant force in order to avoid contacting problems. They are insulated against the screws by a PTFE O-ring. The wires WE, WS, CE and Ref indicate how the cell was connected to the potentiostat (see text). The Pt-wire acts as reference electrode in the three electrode setup.

was 45 wt% for all cells. Humidification of the autoclave atmosphere to prevent the cells from drying was realized by filling the reaction chamber in which the sample holder was mounted with 22.5 ml of a 22.5 wt% KOH solution as shown in Fig. 4. The autoclave was filled with 10 bar N_2, supplied from a gas bottle, before heating. Further pressurization occurred through thermal expansion of the embedded gases and evaporation of part of the solution in the bottom during heating.

2.4. Three electrode setup

A reference electrode was attached to the middle of the FobAEC to determine the oxygen and hydrogen evolution overpotentials η_{O_2} and η_{H_2} as shown in Fig. 5. The hydrogen evolution overpotential was measured in safety gas (9% H_2 in N_2) and the oxygen evolution overpotential in technical air (20% O_2, 80% N_2).

The reaction that takes place at the H_2/Pt/KOH(aq) reference electrode is given in Equation (7) with a standard potential E_C^0 of −0.828 V vs the standard hydrogen electrode, SHE [33].

$$2OH^-(aq) + H_2(g) \leftrightarrow 2H_2O(g) + 2e^- \quad (7)$$

The equilibrium electrode potential vs the SHE for the HER (Reaction 7) E_C^{eq}, under measurement conditions can be calculated from Equation (8), where a_i are activities of species i. For 240 °C and 40 bar it was calculated to be −844 mV under the experimental conditions employed here.

$$E_C^{eq} = E_C^0 + \frac{RT}{2F}\ln\left(\frac{a_{H_2O}^2}{a_{H_2}a_{OH^-}^2}\right) \quad (8)$$

The reaction that takes place at the O_2/Pt/KOH(aq) reference electrode is given in Equation (9) with a standard potential E_A^0 of 0.4 V vs the SHE [33].

$$4OH^-(aq) \leftrightarrow O_2(g) + 2H_2O(g) + 4e^- \quad (9)$$

The equilibrium electrode potential vs the SHE for the OER (Reaction 9) E_A^{eq}, under measurement conditions can be calculated from Equation (10). For 240 °C and 40 bar it was calculated to be 352 mV under the experimental conditions employed here.

$$E_A^{eq} = E_A^0 + \frac{RT}{2F}\ln\left(\frac{a_{O_2}a_{H_2O}^2}{a_{OH^-}^4}\right) \quad (10)$$

3. Results

3.1. Porosimetry analysis

The porosity and pore size distribution of the pellets used for immobilization of the aqueous KOH was characterized by Hg porosimetry and is shown in Fig. 6; the mean pore size was found to be 63 nm with a porosity of 48.0%.

3.2. Scanning electron microscopy

3.2.1. Untreated foam

SEM (Scanning electron microscopy) images of the untreated foam are shown in Fig. 7. The pore size of the nickel and Inconel foam is ca. 450 μm with a porosity of 95% for the nickel foam and >91% for the Inconel foam according to the manufacturer's specification. It can be seen that the surface of the nickel foam is relatively smooth compared to this of the Inconel foam. The coarse layer on the Inconel foam shows the Inconel layer, which has been coated on a nickel foam, similar to those seen on the left part of the figure.

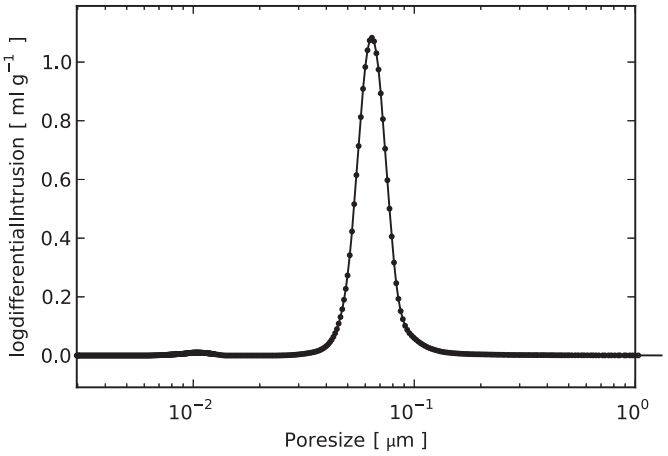

Fig. 6. Results of the mercury intrusion porosimetry of the electrolyte supporting porous $SrTiO_3$ structure showing a mean pore size of 63 nm.

3.2.2. Surface analysis of the FobAECs anode

The porosity of the foam is significantly reduced after pressing of the whole cell body in the uni-axial press. The typical pore size diameter is reduced to values in the order of 150 μm ± 50 μm with an even distribution. The shape is naturally changed to a more flat form instead of being ball-like, as it can be seen in Fig. 8, left image. The highly porous $SrTiO_3$ structure sticks out of the nickel foam at several places up to the surface of the cell. It can be seen that the nickel foam can act as a current collector as well as the active electrode. The right image of Fig. 8 shows the interface of the $SrTiO_3$ and the nickel foam, which will act as the TPB after immersion of the cell into liquid electrolyte. The $SrTiO_3$ has a tendency to form clusters on the surface which have a size of ca. 2–10 μm while the pore size is mainly distributed around 63 nm as shown in Fig. 6.

3.2.3. Surface analysis of the silver deposited anode of the FobAECs

Silver electrodeposition was successfully applied to the nickel foam anode as shown in Fig. 9. The left image shows the foam with silver crystals of a particle size in the region of 10–20 μm and nano sized silver particles distributed all over the foams surface. The right image shows the interface of the same sample at higher magnification where a relatively large silver particle of 7.5 μm can be seen in the upper-left part with well distributed nano sized particles in the range of 50–500 nm.

3.2.4. Cross section analysis of the FobAECs

The results of the cross section analysis are shown in Fig. 10. The brightest structure indicates the metal foams, light grey is the porous $SrTiO_3$ structure and dark grey is the surrounding epoxy coating for the SEM analysis. Both electrodes are pressed out of two layers of the corresponding metal foam. The Inconel foam is less compressed than the nickel foam and shows a higher specific surface area than the pure nickel. It can also be seen that it will be sufficient to use only one layer of Inconel foam, but 2 layers of nickel foam are needed in order to obtain a good distribution of gas channels in combination with the ability of the foam to work as a current collector and active electrode.

3.3. Cell performance at high temperatures

Cell performance tests have mainly been performed at temperatures in the region of 250 °C and pressures around 40 bar. Cyclic voltammograms of different compositions of the FobAECs are shown in Fig. 11. The current density at a polarization of $U_{cell} = 1.5$ V

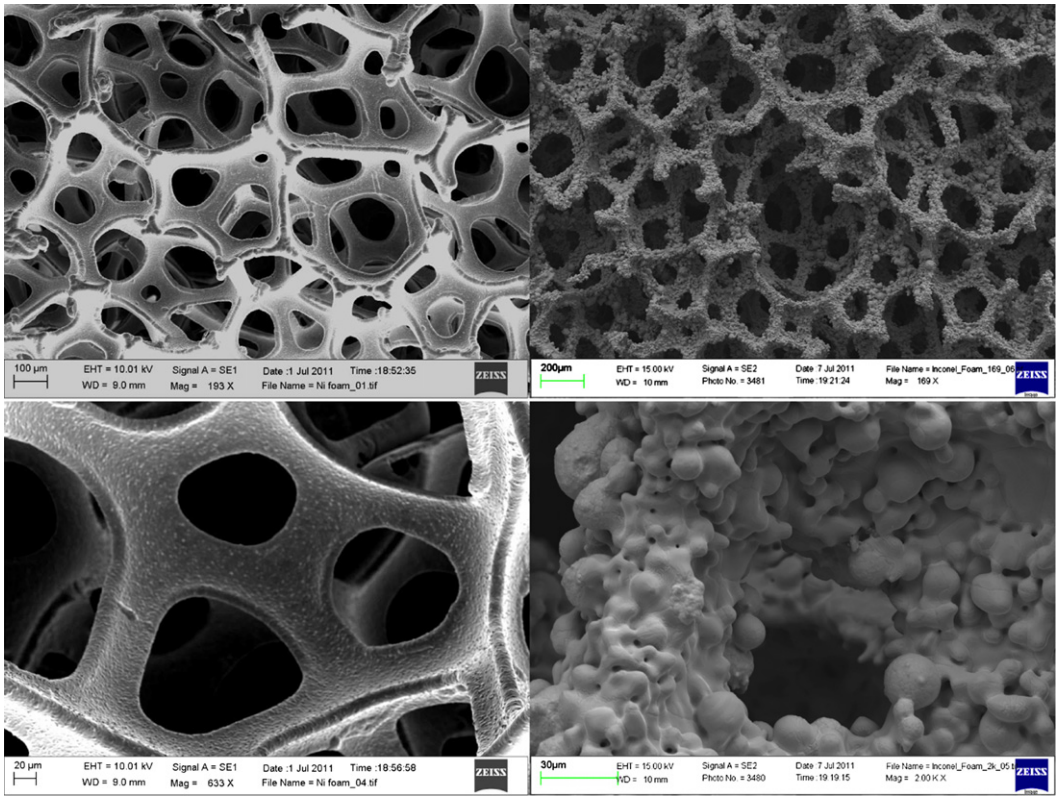

Fig. 7. SEM picture of an untreated nickel foam (upper-left and lower-left) and Inconel foam (upper-right and lower-right). Note: the magnifications are different as indicated by the scale bars.

(uncompensated for ohmic resistance) reached from 466 mA cm^{-2} at 240 °C and 38 bar (for a cell with 2 layers of nickel foam as anode and two layers of Inconel foam as cathode), to 1000 mA cm^{-2} at 240 °C and 37 bar (for a cell with 1 layer of nickel foam with Ag-deposition as anode and one layer of Inconel 625 foam as cathode). Additional performance data for further cell compositions are shown in Table 2. The serial resistance R_s has been measured with EIS under polarization of 1.4 V.

3.4. Ag-deposited nickel anode with Inconel cathode

The Ag-activated cells have shown the best performance as shown in Table 2. Impedance analysis has generally been performed at a polarization voltage of 1.4 V. Fig. 12 shows the cyclic voltammogram for a Ag-activated cell along with polarized impedance measurements before and after recording the voltammogram at polarization voltages of 1.4 V and 1.5 V. The serial resistance R_s decreased slightly after recording the voltammogram from 133 mΩ cm^2 to 125 mΩ cm^2 at 1.4 V polarization, while the area specific resistance of the cell, ASR_{cell}, decreased from 335 mΩ cm^2 before, to 319 mΩ cm^2 after recording the voltammogram. The R_s at 1.5 V was equal to this at 1.4 V (125 mΩ cm^2), whereas the ASR_{cell} reduced to 250 mΩ cm^2. The main change is associated with the low frequency part of the spectrum.

3.5. Influence of the temperature

The performance of a FobAEC with Ag-deposited anode and Inconel cathode at 240 °C and 37 bar, 202 °C and 27 bar and 108 °C and 15 bar in comparison with the corresponding impedance

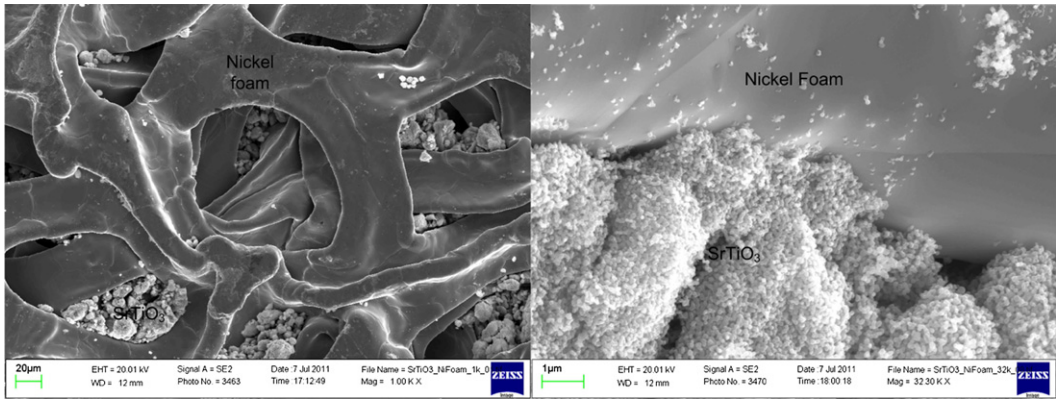

Fig. 8. SEM picture of the surface of the nickel foam anode of a FobAEC at low (left), and high magnification (see scale bar) showing the interface between the nickel foam and the $SrTiO_3$ (right).

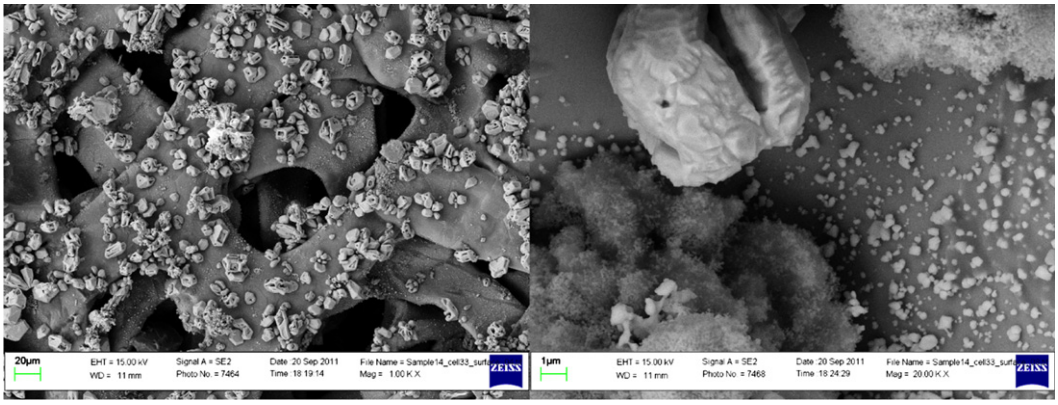

Fig. 9. SEM picture of the surface of the nickel foam after Ag electrodeposition of the anode of a FobAEC at low (left) and high magnification (see scale bar) (right) showing the interface between the nickel foam and $SrTiO_3$ as well as the nano sized Ag particles.

measurements can be seen in Fig. 13. The investigated cell showed current densities of 1000 mA cm^{-2} at 240 °C, 640 mA cm^{-2} at 202 °C and 85 mA cm^{-2} at 108 °C at a cell voltage of 1.5 V (during decreasing the cell voltage). The current densities at 1.75 V were 200 mA cm^{-2}, 1440 mA cm^{-2} and 1940 mA cm^{-2} at temperatures of 108 °C, 202 °C and 240 °C, respectively. The results are not R_s-compensated. The impedance plots at a polarization voltage of 1.4 V show that R_s improved from 164 mΩ cm^2 to 128 mΩ cm^2 and more significantly ASR_{cell} improved from 508 mΩ cm^2 to 361 mΩ cm^2 with increasing temperature from 202 °C to 240 °C as shown in the lower part of Fig. 13. The impedance curve shows significant scattering at low frequencies; a Kramers–Kronig test showed an error above 1% (up to ± 4.5%) at frequencies below 10 Hz with random distribution around zero.

3.6. Determination of the hydrogen evolution overpotential

The overpotential of the Inconel cathode has been studied with the use of the sample holder as shown in Fig. 5. The reference of the potentiostat has been connected to the Pt-wire in the centre of the FobAEC, as shown in Fig. 5 as well, which acts as a reference electrode. The analysis of the hydrogen evolution reaction HER has been performed in safety gas (9% H_2 in N_2) with the results for the cyclic sweep voltammogram shown in Fig. 14. At a current density of 100 mA cm^{-2} the overpotential was −40 mV and at 1000 mA cm^{-2} it was −131 mV, resulting in a Tafel slope of 91 mV dec^{-1}. The uncompensated overpotential for a current density of 1 A cm^{-2} was −0.28 V.

The iR-corrected results (η_{H_2}) correspond to the difference of the cathode potential vs the equilibrium potential of the reference electrode E_C^{eq}. The cathode potential vs the SHE ($E_{C,SHE}$) is displayed on the second ordinate of Fig. 14 (compare Section 2.4).

3.7. Determination of the oxygen evolution overpotential

The oxygen overpotential has been measured for cells with and without the Ag catalyst in technical air (20% O_2, 80% N_2) with the results shown in Fig. 15. The obtained current density for low overpotentials between 50 mV and 150 mV is higher for the not Ag activated cell, which has not generally been the case (compare Fig. 11). At higher overpotentials the situation changes and the current density of the Ag activated anode is higher than that of the pure nickel foam anode, i.e. at a current density of 90 mA cm^{-2} the overpotentials are 250 mV and 220 mV, while at 900 mA cm^{-2} they are 360 mV and 380 mV for the Ag activated anode and the nickel anode, respectively. The Tafel slope for the not activated cell is 160 mV/decade while the Ag-activated anode improved to 130 mV/decade between 90 mA cm^{-2} and 900 mA cm^{-2}. The slope appears to be highly nonlinear.

The iR-corrected results (η_{O_2}) correspond to the difference of the cathode potential vs the equilibrium potential of the reference electrode E_A^{eq}. The anode potential vs the SHE ($E_{A,SHE}$) is displayed on the second ordinate of Fig. 15 (compare Section 2.4).

4. Discussion

4.1. Cell performance

The obtained current densities of 1.0 A cm^{-2} at 1.5 V and 2.0 A cm^{-2} at 1.75 V show that the proposed FobAEC cell design is able to compete with the state of the art PEM (Proton Exchange Membrane) electrolysis cells, but offers cost effective production since no expensive catalysts are needed. High performance has been achieved by increasing the temperature up to 250 °C at

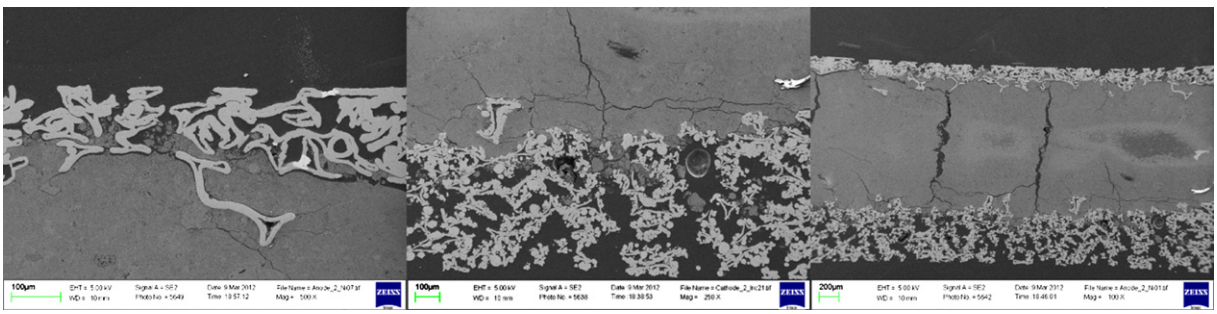

Fig. 10. SEM picture of the cross section of a FobAEC with two layers of nickel and two layers of Inconel foam showing the nickel anode (left), the Inconel cathode (centre) and the full cell (right).

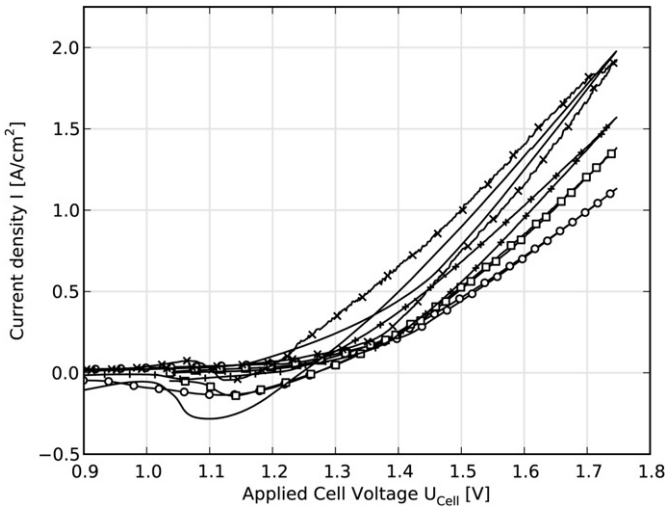

Fig. 11. iV-curves of different cells at temperatures around 240 °C and pressures around 40 bar, i.e.: Cell 3a (×) and Cell 3b (full line) with 1 layer Ag-deposited nickel anode and 1 layer Inconel as cathode; Cell 2 (+) with 1 layer nickel foam anode and 1 layer Inconel as cathode; Cell 1b (□) with 2 layers nickel foam anode and 2 layers Inconel as cathode; Cell 1a (○) with 2 layers nickel foam anode and 2 layers Inconel as cathode.

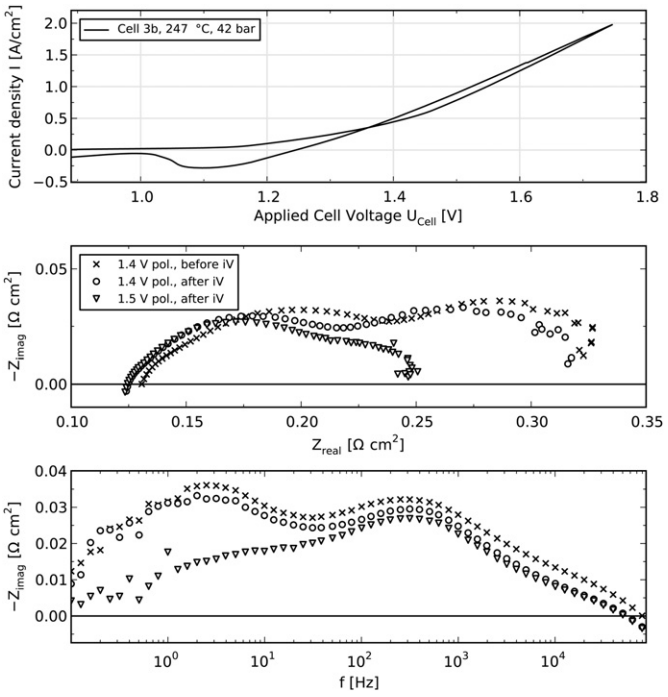

Fig. 12. Cyclic voltammogram (upper figure) of a FobAEC (Cell 3b) with Ag-deposited anode and Inconel cathode at 247 °C and 43 bar in comparison with the corresponding impedance analysis (central figure) at polarization voltages of 1.4 V before (×) and 1.4 V (○) and 1.5 V (▽) after the cyclic voltammetry test.

pressures up to 42 bar. The FobAEC can in principle be used in fuel cell mode as well, but this remains to be proven in future measurements along with long term measurements to determine the stability of the cell.

The overpotential for the HER after iR correction was as low as −40 mV for the Inconel foam at a current density of 100 mA cm^{-2} and −84 mV at a current density of 250 mA cm^{-2} as shown in Fig. 14. A recent review by Zeng and Zang [11] reported values between −58.0 mV and −489 mV for nickel alloys at the same current density of 250 mA cm^{-2}, but lower temperature (70 °C).

Overpotentials for the OER of 224, 235, 250, 270 and 300 mV at a current density of 100 mA cm^{-2} have been reported by Zeng and Zang [11] for Ni + La doped Co_3O_4, Ni + Spinel type Co_3O_4, $La_{0.5}Sr_{0.5}CoO_3$, $Ni_{0.2}Co_{0.8}LaO_3$ and pure nickel electrodes, respectively, at temperatures between 25 °C and 90 °C. These values are similar with the overvoltage measured here at the same current density for the nickel foam anode (225 mV) and the Ag deposited nickel foam anode (254 mV), as shown in Fig. 15. Ag deposition on the anode leads to reduction of the overpotential at elevated current densities.

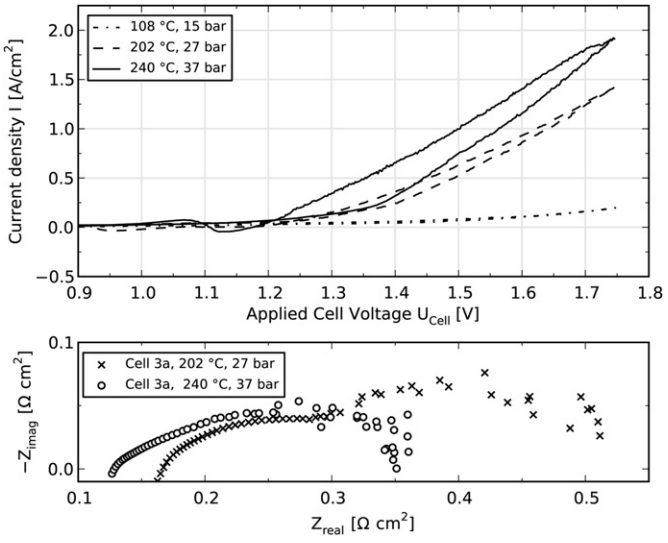

Fig. 13. Cyclic voltammogram (upper figure) of a FobAEC (Cell 3a) with Ag-deposited anode and Inconel cathode at 240 °C and 37 bar (full line), 202 °C and 27 bar (dashed line) and 108 °C and 15 bar (dash-dot) along with the corresponding impedance analysis (lower figure) from data achieved at a polarization of 1.4 V.

4.2. Cell efficiency

The calculation of the efficiency for water or steam electrolysis can be done in several ways, which may lead to confusion when results are compared. The electrical efficiency is often calculated by Equation (11), where $HHV_{H_2,STP}$ is the Higher Heating Value of

Table 2
Comparison of the cell performance for different compositions of the FobAEC at around 240 °C and 40 bar.

Cell	Anode	Cathode	Temperature [°C]/ pressure [bar]	I [mA cm^{-2}] at 1.5 V (uncomp.)	I [mA cm^{-2}] at 1.75 V (uncomp.)	R_s [mΩ cm^2] at 1.4 V polarization	U_{cell} [V] at 0.5 A cm^{-2} (comp.)
Cell 1a	2 layer Ni foam	2 layer Inc foam	240/38	466	1130	148	1.441
Cell 1b	2 layer Ni foam	2 layer Inc foam	237/36	528	1378	140	1.419
Cell 2	1 layer Ni foam	1 layer Inc foam	240/39	679	1570	112	1.388
Cell 3a	1 layer Ni foam + Ag deposition	1 layer Inc foam	240/37	1000	1918	119	1.291
Cell 3b	1 layer Ni foam + Ag deposition	1 layer Inc foam	247/42	903	1978	124	1.337

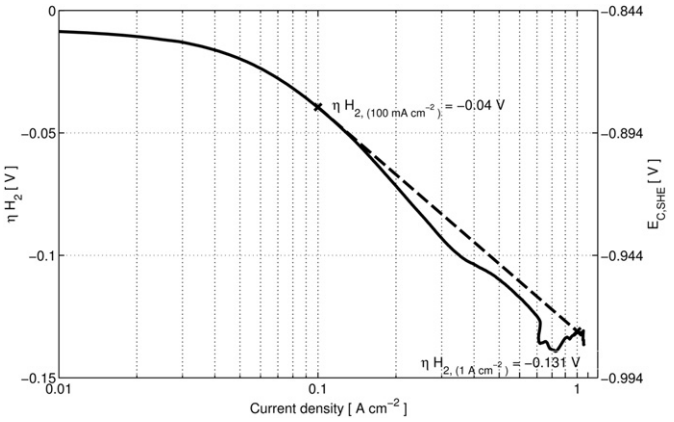

Fig. 14. Current density dependence of the hydrogen evolution overpotential of the Inconel cathode with a sweep rate of 20 mV s^{-1} at 42.1 bar and 248 °C. The full line shows the R_s-compensated applied electrode voltage; the dashed line shows the graphical estimation of the Tafel slope between 100 mA cm^{-2} and 1 A cm^{-2}.

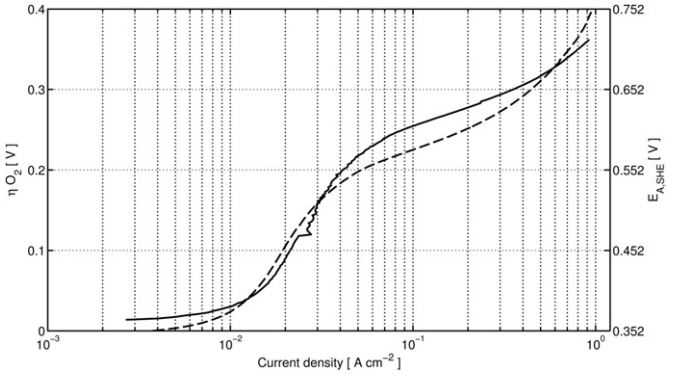

Fig. 15. Current density dependence of the oxygen evolution overpotential of a Ag loaded anode at 43.3 bar and 248 °C (full line) in comparison with the oxygen evolution overpotential of a pure nickel anode (dashed) at 42 bar 250 °C, both recorded with a sweep rate of 50 mV s^{-1} and compensated for R_s.

Hydrogen at standard temperature and pressure, STP; $E_{tn,0}$ is the thermoneutral voltage at STP and U_{Cell} is the applied cell voltage. This can lead to electrical efficiencies greater than 100% since electrolysis is possible at lower voltages starting from 1.23 V at STP as calculated with Equation (6). The energy efficiency is of course below 100%, since the supply of heat is necessary in this case.

$$\eta_{electric} = \frac{HHV_{H_2,STP} n^{-1} F^{-1}}{\text{Electricity demand}} = \frac{E_{tn,0}}{U_{Cell}} = \frac{1.481\ V}{U_{Cell}} \quad (11)$$

Since water electrolysis is usually performed at elevated temperatures, it is more precise to take heat demands into consideration and calculate the efficiency by equation (12), where η_{HHV} is the efficiency correlated to the HHV, $HHV_{H_2,T}$ is the HHV for H_2 at a specific temperature.

$$\eta_{HHV} = \frac{HHV_{H_2,T} n^{-1} F^{-1}}{\text{Electricity demand}} = \frac{E_{tn,T}}{U_{Cell}} \quad (12)$$

The efficiency correlated to the HHV of cell 1a, which reached 1.0 A cm^{-2} at 240 °C and 37 bar, could, if further losses are said to be zero, be calculated to 84.3%. The electric efficiency would be 98.7% at this point.

It is also common to calculate the efficiency against the lower heating value LHV of hydrogen, i.e. the US department of Energy DOE recommends the use of the LHV. Reservations against the use of the LHV have been expressed stating that it is not possible to obtain an efficiency of 100%, although the cell might operate below the thermoneutral voltage, where ohmic losses compensate for the heat demand of the endothermic electrolysis reaction [34]. Anyway, it is of interest to compare the achieved efficiencies against the LHV, as calculated from Equation (13), with the target from the DOE for 2017, which is 74% cell efficiency. The here obtained efficiency η_{LHV} at a current density of 2.0 A cm^{-2} is 70%, while it is 74% at a current density of 1.6 A cm^{-2}.

$$\eta_{LHV} = \frac{\Delta G_f^0 n^{-1} F^{-1}}{\text{Electricity demand}} = \frac{1.229\ V}{U_{Cell}} \quad (13)$$

The influence of the pressure on the reversible cell voltage E_{rev} was discussed in Section 1.2. $E_{rev(t,p)}$ decreases with increasing temperature, but increases with increasing electrolysis pressure, as shown in Fig. 2. The efficiency against $E_{rev(t,p)}$, can be calculated by Equation (14) where $\eta_{E_{rev}(t,p)}$ is the efficiency against the reversible cell voltage $E_{rev(t,p)}$. It is obvious that Equation (14) is the only one taking the system pressure into account (compare Fig. 2) and allows for comparison of cells operated at elevated pressures, although the same restrictions as discussed for η_{LHV} are valid for $\eta_{E_{rev}(t,p)}$.

$$\eta_{E_{rev}(t,p)} = \frac{E_{rev(t,p)}}{U_{Cell}} \quad (14)$$

Table 3
Efficiencies of the measured cells at relevant current densities in comparison with available literature data.

Cell/type	Temperature [°C]/pressure [bar]	I [mA cm^{-2}]	U_{cell} [V]	$\eta_{electric}$	η_{LHV}	η_{HHV}	$\eta_{Erev(t,p)}$
Cell 3a; Ag deposited Ni foam anode, Inconel cathode	108/15	100	1.57	94.3	78.3	80.1	75.6
		200	1.75	84.6	70.2	71.9	67.8
	202/27	100	1.27	116.6	96.8	99.4	92.5
		200	1.33	111.4	92.4	94.9	88.4
		500	1.45	102.1	84.8	87.1	81.1
		1000	1.62	91.4	75.9	77.9	72.5
	240/37	100	1.22	121.4	100.7	103.6	96.0
		200	1.25	118.5	98.3	101.1	93.7
		500	1.35	109.7	91.0	93.6	86.8
		1000	1.5	98.7	81.9	84.3	78.1
		2000	1.76	84.1	69.8	71.8	66.6
Raney-nickel cell [3]	100/4	400	1.55	95.5	79.3	94.8	75.3
Anode: NiFe(OH)2 layer. Cathode: Pt coated SS [36]	58/atmospheric	1000	2.12	69.9	58.0	69.3	55.0
Polished nickel electrodes in 50 wt% KOH [5]	264/15.5	500	1.55 (iR-corrected)	95.5	79.3	81.6	74.7
		1000	1.65 (iR-corrected)	89.8	74.5	76.7	70.1

Furthermore it should be stressed that none of the given equations is utilizable to compare the performance of a cell unless the current density is also given. The efficiency of the measured cells have been calculated in comparison with cells from the literature at relevant current densities and are shown in Table 3. The differences between the calculated efficiencies by Equation (11)–(14) are up to 25% for the same data-set (compare Cell 1a at 240 °C and 37 bar).

4.3. System costs

No precious materials are used in the cell, and metal foams are widely used in industrial processes. Thus, it is possible to produce FobAECs at raw material prices under 1310 US$ m^{-2}, equal to 88 US$ kW_{el}^{-1} if operated at 1.0 A cm^{-2} and no further electro-catalysts are used. Ag is expensive material, but if it is used as a catalyst only with a small load, it would not raise the cost very much, especially if compared to some of the best known catalysts for the OER (RuO_2 or IrO_2) [35]. Lab-scale prices for Ag, RuO_2 and IrO_2 are 5.00 US$ g^{-1}, 34.40 US$ g^{-1} and 91.40 US$ g^{-1}, respectively (Alfa Aesar, October 2012). The price of silver on the stock market is ca. 1 US$ g^{-1} as of October 2012, whereas platinum cost about 50 US$ g^{-1}. The additional investment costs of an electrolysis system using FobAECs due to the high temperature and pressure will be compensated by the fact that the systems can be build much smaller if compared to standard alkaline electrolysis systems at the same production rate due to the high current densities and a high electrical efficiency. Also the costs of pressurized hydrogen (and oxygen) will be reduced.

5. Conclusion

A new type of alkaline electrochemical cell has been developed and tested. Current densities of almost 1.0 A cm^{-2} at 240 °C and 37 bar have been reached at the thermoneutral voltage for water splitting (1.481 V at STP), thereby achieving an electrical efficiency of 98.7% at this current density. At the industrial more relevant cell voltage of 1.75 V (industrial electrolysis systems are usually operated at or above this voltage, compare Table 5 from Ref. [11]), corresponding to an electrical efficiency of 84.5%, the current density reached 2.0 A cm^{-2} and is thereby better than the targets of the US Department of Energy DOE for 2017.

Acknowledgements

The financial support from the 2nd generation alkaline electrolysis project, EUDP 63011-0200, is gratefully acknowledged. The authors are also thankful for additional financial support from the “Catalysis for Sustainable Energy initiative”, funded by the Danish Ministry of Science, Technology and Innovation. Furthermore we are thankful for the supply of metal foams by Alantum Germany GmbH. Johan Hjelm is acknowledged for valuable consultation during the electrodeposition experiments. For valuable discussions along the way, we are very thankful to Jonathan Hallinder. We also appreciate the consultations from Sune D. Ebbesen and Ane Sælland Christiansen.

References

[1] H. Wendt, H. Hofmann, V. Plzak, Materials Chemistry and Physics 22 (1–2) (1989) 27–49.
[2] Ø. Ulleberg, T. Nakken, A. Eté, International Journal of Hydrogen Energy 35 (5) (2010) 1841–1852.
[3] J. Divisek, P. Malinowski, J. Mergel, H. Schmitz, International Journal of Hydrogen Energy 13 (3) (1988) 141–150.
[4] K. Onda, T. Kyakuno, K. Hattori, K. Ito, Journal of Power Sources 132 (1–2) (2004) 64–70.
[5] M.H. Miles, G. Kissel, P.W.T. Lu, S. Srinivasan, Journal of the Electrochemical Society 123 (3) (1976) 332–336.
[6] J. Fischer, H. Hofmann, G. Luft, H. Wendt, AIChE Journal 26 (5) (1980) 794–802.
[7] H. Wendt, H. Hofmann, International Journal of Hydrogen Energy 10 (6) (1985) 375–381.
[8] O. Ulleberg, International Journal of Hydrogen Energy 28 (1) (2003) 21–33.
[9] D. Pletcher, X. Li, International Journal of Hydrogen Energy 36 (23) (2011) 15089–15104.
[10] F. Allebrod, C. Chatzichristodoulou, P.L. Mollerup, M.B. Mogensen, International Journal of Hydrogen Energy 37 (21) (2012a) 16505–16514.
[11] K. Zeng, D. Zhang, Progress in Energy and Combustion Science 36 (3) (2010) 307–326.
[12] C.W. Bale, P. Chartrand, S.A. Degterov, G. Eriksson, K. Hack, R.B. Mahfoud, J. Melançon, A.D. Pelton, S. Petersen, Calphad 26 (2) (2002) 189–228.
[13] J. Balej, International Journal of Hydrogen Energy 10 (4) (1985) 233–243.
[14] J. Balej, International Journal of Hydrogen Energy 10 (6) (1985) 365–374.
[15] R. Knibbe, A. Hauch, J. Hjelm, S.D. Ebbesen, M. Mogensen, Green 16 (2011) 141–169.
[16] G. Kreysa, H.J. Kuelps, Journal of the Electrochemical Society 128 (5) (1981) 979–984.
[17] P.S. Jørgensen, K.V. Hansen, R. Larsen, J.R. Bowen, Journal of Power Sources 195 (24) (2010) 8168–8176.
[18] J. Balej, International Journal of Hydrogen Energy 10 (2) (1985c) 89–99.
[19] S. Trasatti, Electrochimica Acta 29 (11) (1984) 1503–1512.
[20] J.K. Nørskov, T. Bligaard, A. Logadottir, J.R. Kitchin, J.G. Chen, S. Pandelov, U. Stimming, Journal of the Electrochemical Society 152 (3) (2005) J23–J26.
[21] L.A. Kibler, ChemPhysChem 7 (5) (2006) 985–991.
[22] E. Gülzow, N. Wagner, M. Schulze, Fuel Cells 3 (1–2) (2003) 67–72.
[23] M.A. Kostowskyj, R.J. Gilliam, D.W. Kirk, S.J. Thorpe, International Journal of Hydrogen Energy 33 (20) (2008) 5773–5778.
[24] M. Hamdani, R.N. Singh, P. Chartier, International Journal of Electrochemical Science 5 (4) (2010) 556–577.
[25] J. Divisek, H. Schmitz, J. Balej, Journal of Applied Electrochemistry 19 (4) (1989) 519–530.
[26] J. Banhart, Progress in Materials Science 46 (6) (2001) 559–632.
[27] F. Bidault, D.J.L. Brett, P.H. Middleton, N. Abson, N.P. Brandon, International Journal of Hydrogen Energy 34 (16) (2009) 6799–6808.
[28] M. Gerber, R. Poss, A. Tillmann, G. Walther, B. Kieback, K. Wolf, F. Hanel, Journal of Sandwich Structures and Materials 14 (2) (2012) 181–196.
[29] F. Allebrod, C. Chatzichristodoulou, P.L. Mollerup, M.B. Mogensen, High Performance Reversible Electrochemical Cell for H_2O Electrolysis or Conversion of CO_2 and H_2O to Fuel, Patent Pending No. 12164019.7-2119, 2012.
[30] S. Guo, D. Li, Q. Guo, Z. Wu, H. Peng, J. Hu, Journal of Materials Science. ISSN: 00222461 47 (15) (2012). ISSN: 00222461 5867–5878.
[31] C. Graves, RAVDAV Data Analysis Software, Version 0.9.7 (2012).
[32] F.W. Pement, I.L.W. Wilson, R.G. Aspden, Materials Performance 19 (4) (1980) 43–49.
[33] CRC Handbook of Chemistry and Physics: A Ready-reference Book of Chemical and Physical Data, CRC Press, Boca Raton, FL, 2011, ISBN 1439855110.
[34] S.D. Ebbesen, S.H. Jensen, A. Hauch, M.Mogensen, HighTemperature Electrolysis, submitted for publication.
[35] H.J. Miao, D.L. Piron, Journal of Applied Electrochemistry 21 (1) (1991) 55–59.
[36] X. Li, F.C. Walsh, D. Pletcher, Physical Chemistry Chemical Physics 13 (3) (2011) 1162–1167.